

## Hydrogenation Catalysis

International Edition: DOI: 10.1002/anie.201508107  
German Edition: DOI: 10.1002/ange.201508107

## Synthesis of Supported Ultrafine Non-noble Subnanometer-Scale Metal Particles Derived from Metal–Organic Frameworks as Highly Efficient Heterogeneous Catalysts

Xinchen Kang, Huizhen Liu, Minqiang Hou, Xiaofu Sun, Hongling Han, Tao Jiang, Zhaofu Zhang, and Buxing Han\*

**Abstract:** The properties of supported non-noble metal particles with a size of less than 1 nm are unknown because their synthesis is a challenge. A strategy has now been created to immobilize ultrafine non-noble metal particles on supports using metal–organic frameworks (MOFs) as metal precursors. Ni/SiO<sub>2</sub> and Co/SiO<sub>2</sub> catalysts were synthesized with an average metal particle size of 0.9 nm. The metal nanoparticles were immobilized uniformly on the support with a metal loading of about 20 wt %. Interestingly, the ultrafine non-noble metal particles exhibited very high activity for liquid-phase hydrogenation of benzene to cyclohexane even at 80 °C, while Ni/SiO<sub>2</sub> with larger Ni particles fabricated by a conventional method was not active under the same conditions.

Supported nanocatalysts have been widely studied based on their high activity for different chemical reactions.<sup>[1]</sup> The size of metal particles is one of the most important factors that dictate the catalytic performance.<sup>[2]</sup> Various routes for synthesizing supported nanocatalysts with metal particle size of less than 1 nm to 2 nm have been explored.<sup>[3]</sup> However, most of the reported ultrafine metal particles were noble metal particles,<sup>[4]</sup> and immobilization of ultrafine non-noble metal particles on supports is challenging.

Catalytic hydrogenation of benzene to cyclohexane is an important reaction in the chemistry industry. The reaction usually requires harsh conditions because of the high stabilization energy of benzene resulting from aromaticity. The catalytic activity of heterogeneous metal catalysts for the hydrogenation of benzene decreases in the order of Rh > Ru > Pt > Ni.<sup>[5]</sup> Supported Rh, Ru, and Pt metal catalysts can catalyze liquid-phase benzene hydrogenation with high activity.<sup>[6]</sup> However, the high price and low reserve of noble metals limit their application. Benzene hydrogenation is usually conducted at above 150 °C over supported non-noble Ni catalysts under gas-phase conditions and at lower turnover frequency.<sup>[7]</sup> In many cases, liquid-phase hydrogenation has economical advantages in terms of capital costs and energy consumption.<sup>[8]</sup> Benzene hydrogenation in the liquid phase using non-noble catalysts at lower temperature is highly

desirable. The supported non-noble metal catalysts such as Ni and Co with a particle size less than 1 nm may be efficient for the reaction at lower temperatures, which is unknown because synthesis of ultrafine nanocatalysts is a great challenge.

Metal–organic frameworks (MOFs) have attracted significant attention.<sup>[9]</sup> They are potential materials for gas storage, separation, catalysis, biomedicine, chromatography, and sensing.<sup>[10]</sup> MOFs can also be used as precursors to synthesize other materials, such as carbon materials and oxides,<sup>[11]</sup> as well as composites.<sup>[12]</sup> However, using MOFs as precursors to synthesize supported metal catalysts has not been reported. Herein, we proposed a new strategy to use MOFs as precursors to synthesize ultrafine non-noble metal particles immobilized on SiO<sub>2</sub> supports. Ni/SiO<sub>2</sub> and Co/SiO<sub>2</sub> catalysts were synthesized using this method with Ni or Co average particle size of less than 1 nm, which exhibited very high activity and stability for the liquid-phase hydrogenation of benzene below 100 °C.

The proposed method to synthesize ultrafine metal particles on the SiO<sub>2</sub> is shown in Figure 1, which is discussed briefly taking the synthesis of Ni/SiO<sub>2</sub> as example, and the details are given in the experimental section (see the Supporting Information). In the experiment, the mixed solvent consisting of ionic liquid (IL) 1-octyl-3-methylimidazolium perchlorate (OmimClO<sub>4</sub>, the structure is shown in the

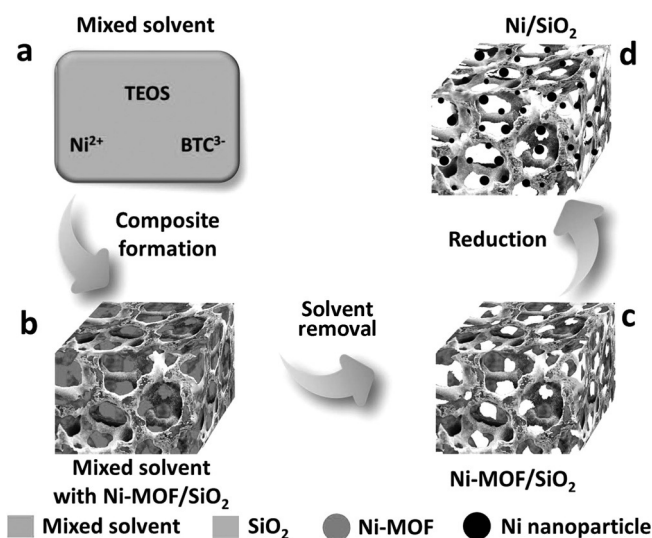


Figure 1. The route for the synthesis of the Ni/SiO<sub>2</sub> catalysts.

\*X. C. Kang, Prof. H. Z. Liu, Dr. M. Q. Hou, X. F. Sun, H. L. Han, Prof. T. Jiang, Dr. Z. F. Zhang, Prof. B. X. Han  
Beijing National Laboratory for Molecular Sciences  
Institute of Chemistry, Chinese Academy of Sciences (China)  
E-mail: hanbx@iccas.ac.cn

Supporting information for this article is available on the WWW under <http://dx.doi.org/10.1002/anie.201508107>.

Supporting Information, Figure S1), triethylammonium nitrate, and water were prepared. Then tetraethoxysilane (TEOS, precursor of  $\text{SiO}_2$ ), 1,3,5-benzenetricarboxylic acid ( $\text{H}_3\text{BTC}$ ) and  $\text{Ni}(\text{NO}_3)_2$  (precursors of the Ni-MOF) were charged into the mixed solvent and a homogeneous solution was formed because the mixed solvent can dissolve both organic and inorganic precursors (Figure 1 a). Ni-MOF and  $\text{SiO}_2$  formed gradually by the coordination reaction and hydrolysis reaction, respectively. Therefore, the Ni-MOF crystals were embedded in the  $\text{SiO}_2$  framework together with some solvent (Figure 1 b). Ni-MOF/ $\text{SiO}_2$  composites were obtained after washing and drying to remove the solvent (Figure 1 c). Then, the obtained Ni-MOF/ $\text{SiO}_2$  composites were dispersed in 50 wt % DMF aqueous solution and the  $\text{Ni}^{2+}$  ions in the Ni-MOF were reduced by  $\text{NaBH}_4$  under a  $\text{N}_2$  atmosphere, and the metallic Ni clusters were immobilized on the  $\text{SiO}_2$ . Meanwhile the  $\text{BTC}^{3-}$  ligands were dissolved in the DMF solution. The Ni/ $\text{SiO}_2$  catalysts were obtained after washing and drying (Figure 1 d). In this novel route, the reduction of  $\text{Ni}^{2+}$  occurs at Ni-MOF/liquid interphase, and therefore the rate was slow. Furthermore, the Ni-MOF particles were trapped in the  $\text{SiO}_2$  framework, and the reduction took place close to the surface of  $\text{SiO}_2$ . Moreover, the porous structure of  $\text{SiO}_2$  offered sufficient sites for Ni nanoparticles to attach. These unique features are favorable to immobilizing ultrafine Ni particles on the supports.

The X-ray diffraction (XRD) pattern of the Ni-MOF/ $\text{SiO}_2$  composites is shown in the Supporting Information, Figure S2. All of the peaks in the XRD pattern of the composites agree well with the reported bulk phase of  $\text{Ni}_3(\text{BTC})_2 \cdot 12\text{H}_2\text{O}$  (Ni-MOF).<sup>[13]</sup> The composites had typical micropores of Ni-MOFs entered at about 0.6 nm as determined by  $\text{N}_2$  adsorption/desorption method (Supporting Information, Figure S3). All these indicated that Ni-MOF existed in the Ni-MOF/ $\text{SiO}_2$  composites. The  $\text{N}_2$  adsorption/desorption isotherms and mesopore size distribution of the Ni-MOF/ $\text{SiO}_2$  are shown in the Supporting Information, Figure S4, and the BET surface area, total pore volume, and average pore size are listed in Table S1. The mesopore size distribution curve of the Ni-MOF/ $\text{SiO}_2$  had a peak centered at about 5 nm, which resulted from the removal of the entrained solvent from steps b to c in Figure 1.

The scanning electron microscope (SEM) image of the as-synthesized Ni/ $\text{SiO}_2$  is shown in Figure 2 a. The size of the Ni/ $\text{SiO}_2$  was in the range of 5–10  $\mu\text{m}$ . The transmission electron microscopy (TEM) image and high-angle annular bright-field (HAABF) image from scanning transmission electron microscopy (STEM) of the Ni/ $\text{SiO}_2$  are shown in Figures 2 b and 2 c, respectively. The Ni nanoparticles were immobilized uniformly on the  $\text{SiO}_2$  supports with an average size of 0.9 nm, and the Ni loading determined by ICP-AES (VISTA-MPX) was 21 wt %. The particle size distribution is demonstrated in Figure 2 d, which shows that most of Ni particles have the size of less than 1 nm. The size of the Ni nanoparticles calculated by Scherrer equation from XRD pattern shown in Figure 2 e is about 1 nm, which corresponds well with the TEM result. The X-ray photoelectron spectrum (XPS) for Ni 2p is shown in Figure 2 f. The characteristic Ni 2p peaks are associated with  $\text{Ni}(\text{OH})_2$  and Ni, respectively.<sup>[14]</sup> On the surface of the

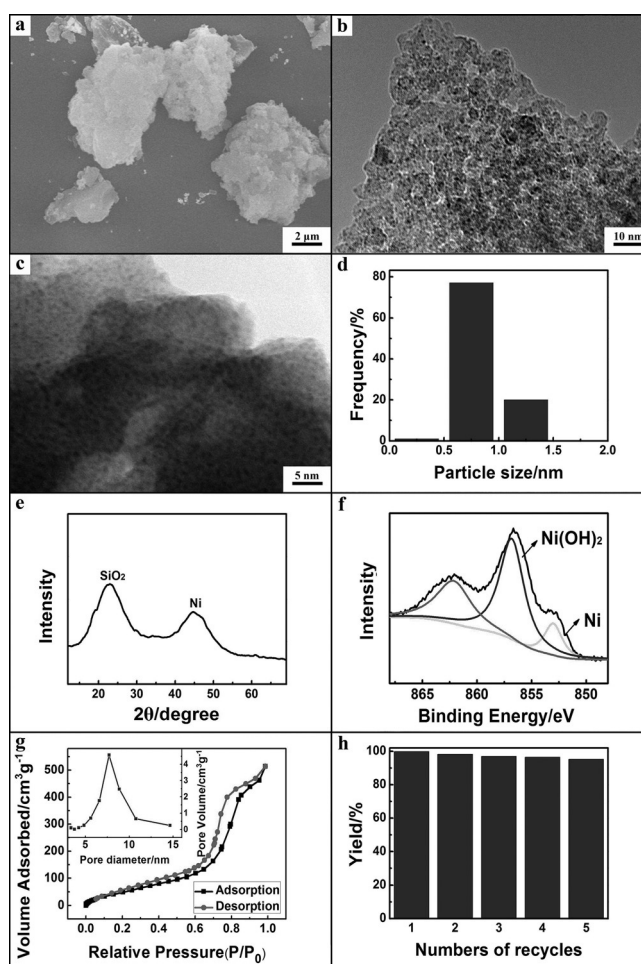


**Figure 2.** Related characterizations of the Ni/ $\text{SiO}_2$ : a) SEM image, b) TEM image, c) HAABF-STEM image, d) particle size distribution, e) XRD pattern, f) XPS spectrum of Ni 2p, g)  $\text{N}_2$  adsorption/desorption isotherms and (inset) mesopore size distribution, and h) reusability for benzene hydrogenation to cyclohexane under the condition given as entry 1 in Table 1. The Ni loading was 21 wt % as determined by ICP-AES.

catalyst, some Ni atoms existed as  $\text{Ni}^0$ , and most of them were oxidized. The fractal structure of the Ni/ $\text{SiO}_2$  was analyzed by small-angle X-ray scattering (SAXS). It was found that mass fractal existed in the Ni/ $\text{SiO}_2$  and the fractal dimension  $D_m$  was 1.97 (Supporting Information, Figure S5), indicating the Ni/ $\text{SiO}_2$  had very loose structure,<sup>[15]</sup> which agrees with the porous and loose structure observed from the TEM image (Figure 2 b). Figure 2 g shows  $\text{N}_2$  adsorption/desorption isotherms and mesopore size distribution of Ni/ $\text{SiO}_2$ ; the BET surface area, total pore volume, and average pore size are shown in the Supporting Information, Table S1. The mesopore size distribution curve has a peak centered at about 8 nm, which was larger than that of Ni-MOF/ $\text{SiO}_2$  composites. The enlarged pore size derives from the removed Ni-MOF particles, further confirming that the Ni-MOF particles in the Ni-MOF/ $\text{SiO}_2$  composites were trapped in the  $\text{SiO}_2$  framework.

We also prepared Co/ $\text{SiO}_2$  using the same method. Similarly, the Co/ $\text{SiO}_2$  was synthesized via Co-MOF/ $\text{SiO}_2$  as

precursor. The XRD pattern (Supporting Information, Figure S6) agrees well with that reported bulk phase of  $\text{Co}_3(\text{BTC})_2 \cdot 12\text{H}_2\text{O}$  (Co-MOF),<sup>[16]</sup> and the micropores centered at 0.6 nm further confirmed the existence of MOF particles in the composites as well (Supporting Information, Figure S7). The BET data of Co-MOF/SiO<sub>2</sub> is shown in Figure S8 and Table S1. The related characterizations such as TEM, HAABF-STEM, particle size distribution, XPS, XRD pattern, and N<sub>2</sub> adsorption/desorption isotherms of the as-synthesized Co/SiO<sub>2</sub> are shown in Figure 3 and the Supporting

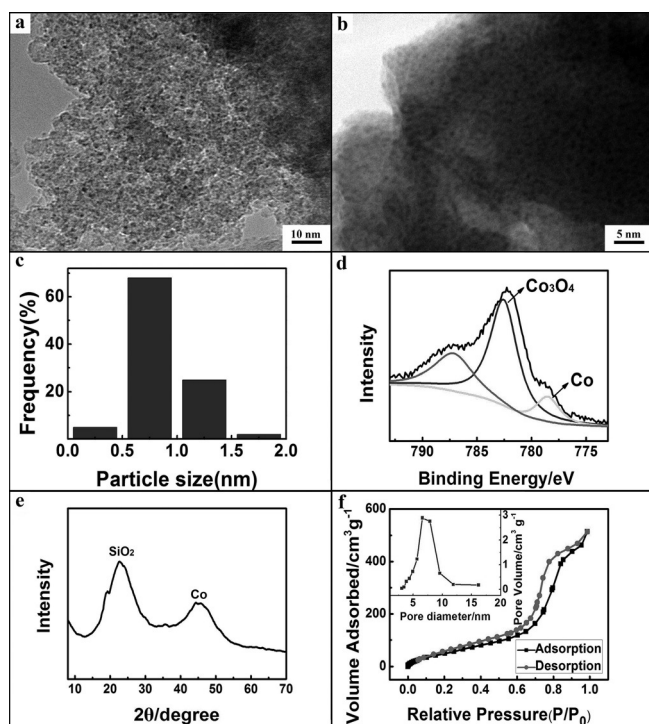


**Figure 3.** Related characterizations of Co/SiO<sub>2</sub>: a) TEM image, b) HAABF-STEM image, c) particle size distribution, d) XPS spectrum of Co 2p, e) XRD pattern, and f) N<sub>2</sub> adsorption/desorption isotherms and mesopore size distribution (inset).

Information, Table S1. The characteristics of the Co/SiO<sub>2</sub> were similar to those of Ni/SiO<sub>2</sub>. In particular, the Co nanoparticles with average particle size of <1 nm were immobilized uniformly on the SiO<sub>2</sub> supports with the Co loading of 19 wt % determined by ICP-AES. The two peaks in XPS spectrum are associated with Co<sub>3</sub>O<sub>4</sub> and Co<sup>0</sup>, respectively.<sup>[17]</sup>

Herein, we studied the catalytic performances of the Ni/SiO<sub>2</sub> and Co/SiO<sub>2</sub> catalysts for benzene hydrogenation to cyclohexane in the liquid phase under solvent-free conditions, and the results are listed in Table 1. It can be known from Table 1 that the Ni/SiO<sub>2</sub> and Co/SiO<sub>2</sub> showed excellent activity for the reaction at 80 °C and 100 °C. For comparison, we carried out the reaction catalyzed by Ni/SiO<sub>2</sub> catalysts prepared by conventional impregnation method using Ni(NO<sub>3</sub>)<sub>2</sub> as precursor and SiO<sub>2</sub> as support.<sup>[18]</sup> The detailed procedures to prepare the catalysts are discussed in the experimental section. The TEM images of the Ni/SiO<sub>2</sub>

catalysts with different Ni loadings of 5 wt %, 10 wt %, and 21 wt % prepared by conventional impregnation method are shown in the Supporting Information, Figure S9. The average particle size of different catalysts (Table 1) increased with the increase of the Ni loading. The catalysts with large Ni particle size exhibited very low catalytic activity for benzene hydrogenation at 100 °C and had no activity at 80 °C (Table 1, entries 7 and 8). Actually, benzene hydrogenation using Ni catalysts is usually carried out at the temperature higher than 150 °C under gas-phase conditions,<sup>[7]</sup> which further confirms that the Ni and Co catalysts with particle size less than 1 nm had extremely high activity. The surface active metal atoms of all the catalysts were determined by chemisorption method as previously reported,<sup>[19]</sup> and the results are listed in Table 1. The number of surface active metal atoms increased with decreasing size of the nanoparticles. The main reason is that smaller particles had more oxidized metal atoms as shown by the XPS spectra (Figure 2f; Supporting Information, Figure S10), which are not active compared with the larger particles. The turnover frequency (TOF) at low benzene conversion (20 %) based on the surface active metal atoms was calculated.<sup>[19]</sup> It can be seen from Table 1 that the TOF of the Ni/SiO<sub>2</sub> catalysts with particle size of less than 1 nm was much larger than that of the Ni/SiO<sub>2</sub> catalysts with larger particle size. Furthermore, the TOF based on active metal of Ni nanoparticles is larger than that of Co nanoparticles with similar size, illustrating that Ni is a more active hydrogenation catalyst than Co. Moreover, the study of reusability of the Ni/SiO<sub>2</sub> catalysts with a particle size of less than 1 nm indicated that the catalysts can be used at least five times without obvious change of the activity (Figure 2h), and the TEM image and XPS spectrum of the Ni/SiO<sub>2</sub> catalysts after used five times are shown in Figure S11. It can be seen that the size of the Ni nanoparticles were nearly the same as that in the virgin catalyst. Some Ni atoms existed in Ni<sup>0</sup> state and most of them were oxidized.

There are at least two factors that are favorable to having high activity of the catalysts. First, the ultrafine metal particles offer sufficient active centers and have higher surface energy based on the low-coordination and unsaturated atoms,<sup>[20]</sup> which may play an important role for the high activity at lower temperature. Second, the SiO<sub>2</sub> supports were porous which benefits for reactants adsorption and mass transfer. Exploration of the detailed mechanism for the phenomenon that ultrafine Ni and Co particles are very active for the reaction at lower temperature is very interesting, and needs to be studied further.

In summary, we proposed a novel strategy for synthesizing non-noble metal catalysts supported on porous SiO<sub>2</sub> using MOFs as metal precursors, and Ni/SiO<sub>2</sub> and Co/SiO<sub>2</sub> catalysts were prepared by this method. In the catalysts, the metal nanoparticles with average size of less than 1 nm were immobilized uniformly on the porous supports with metal loading of about 20 wt %. The catalysts prepared exhibited excellent activity and stability for benzene hydrogenation to cyclohexane in liquid phase below 100 °C. In contrast, the Ni/SiO<sub>2</sub> with larger Ni particles fabricated by conventional method was not active at the same condition. We believe that the cheap and highly active catalysts have great potential of

**Table 1:** Catalytic performances of Ni/SiO<sub>2</sub> and Co/SiO<sub>2</sub> catalysts for benzene hydrogenation to cyclohexane.<sup>[a]</sup>

Entry	Catalyst	Average particle size [nm]	Metal loading [%] <sup>[b]</sup>	Surface-active metal atoms [%] <sup>[c]</sup>	T [°C]	P [MPa]	t [h]	Yield [%]	TOF <sub>1</sub> [h <sup>-1</sup> ] <sup>[d]</sup>	TOF <sub>2</sub> [h <sup>-1</sup> ] <sup>[e]</sup>
1	Ni/SiO <sub>2</sub> <sup>[f]</sup>	<1 m	21	0.1511	100	8	1.8	>99	132.1	18359.4
2	Ni/SiO <sub>2</sub> <sup>[f]</sup>	<1 m	21	0.1511	100	6	3	>99	90.1	12522.2
3	Ni/SiO <sub>2</sub> <sup>[f]</sup>	<1 m	21	0.1511	80	8	9	>99	28.6	3974.9
4	Ni/SiO <sub>2</sub> <sup>[f]</sup>	<1 m	21	0.1511	80	6	15	>99	18.5	2571.1
5	Co/SiO <sub>2</sub> <sup>[g]</sup>	<1 m	19	0.4778	100	8	3.0	>99	84.3	3352.2
6	Co/SiO <sub>2</sub> <sup>[g]</sup>	<1 m	19	0.4778	100	6	6.5	>99	40.4	1606.5
7	Ni/SiO <sub>2</sub> <sup>[h]</sup>	7.9	21	3.7292	100	8	5	31	15.8	89.0
8	Ni/SiO <sub>2</sub> <sup>[h]</sup>	7.9	21	3.7292	80	8	5	0	0	0
9	Ni/SiO <sub>2</sub> <sup>[h]</sup>	4.7	5	0.2921	100	8	5	20	36.3	621.4
10	Ni/SiO <sub>2</sub> <sup>[h]</sup>	6.1	10	0.7026	100	8	5	28	24.0	341.6

[a] Reaction conditions: 3.0 g benzene, 0.05 g catalysts, solvent free. [b] The metal loading was determined by ICP-AES (VISTA-MPX). [c] The surface active metal atoms was determined by chemisorption method. [d] TOF<sub>1</sub> was calculated as moles of converted benzene per mole of metal per hour after 20% benzene conversion.<sup>[19]</sup> [e] TOF<sub>2</sub> was calculated as moles of converted benzene per mole of surface active metal atoms per hour after 20% benzene conversion.<sup>[19]</sup> [f] Ni/SiO<sub>2</sub> catalysts synthesized by the route proposed herein (Figure 2). [g] Co/SiO<sub>2</sub> catalysts synthesized by the route proposed herein (Figure 3). [h] Ni/SiO<sub>2</sub> catalysts synthesized by conventional impregnation method using Ni(NO<sub>3</sub>)<sub>2</sub> as precursor (Supporting Information, Figure S9).

application, and the novel strategy provides new opportunities for synthesizing low-cost and high-performance ultrafine non-noble metal catalysts.

## Acknowledgements

The authors thank the National Natural Science Foundation of China (21133009, 21173239, U1232203, 21321063), the Ministry of Science and Technology of China (2011CB808603), and the Chinese Academy of Sciences (KJJCX2.YWH30). The SAXS experiments were carried out at Beijing Synchrotron Radiation Facility.

**Keywords:** benzene hydrogenation · metal-organic frameworks · non-noble metals · supported catalysts · ultrafine nanoparticles

**How to cite:** *Angew. Chem. Int. Ed.* **2016**, *55*, 1080–1084  
*Angew. Chem.* **2016**, *128*, 1092–1096

- [1] a) M. Stratakis, H. Garcia, *Chem. Rev.* **2012**, *112*, 4469–4506; b) W. T. Yu, M. D. Porosoff, J. G. G. Chen, *Chem. Rev.* **2012**, *112*, 5780–5817; c) Y. Zhang, X. J. Cui, F. Shi, Y. Q. Deng, *Chem. Rev.* **2012**, *112*, 2467–2505; d) J. L. Gong, H. R. Yue, Y. J. Zhao, S. Zhao, L. Zhao, J. Lv, S. P. Wang, X. B. Ma, *J. Am. Chem. Soc.* **2012**, *134*, 13922–13925; e) X. B. Peng, K. Cheng, J. C. Kang, B. Gu, X. Yu, Q. H. Zhang, Y. Wang, *Angew. Chem. Int. Ed.* **2015**, *54*, 4553–4556; *Angew. Chem.* **2015**, *127*, 4636–4639; f) J. Carrasco, D. Lopez-Durán, Z. Y. Liu, T. Duchoñ, J. Evans, S. D. Senanayake, E. J. Crumlin, V. Matolín, J. A. Rodríguez, M. V. Ganduglia-Pirovano, *Angew. Chem. Int. Ed.* **2015**, *54*, 3917–3921; *Angew. Chem.* **2015**, *127*, 3989–3993.
- [2] a) M. S. Chen, D. W. Goodman, *Science* **2004**, *306*, 252–255; b) M. Turner, V. B. Golovko, O. P. H. Vaughan, P. Abdulkhan, A. Berenguer-Murcia, M. S. Tikhov, B. F. G. Johnson, R. M. Lambert, *Nature* **2008**, *454*, 981–983.
- [3] a) S. F. Hackett, R. M. Brydson, M. H. Gass, I. Harvey, A. D. Newman, K. Wilson, A. F. Lee, *Angew. Chem. Int. Ed.* **2007**, *46*, 8593–8596; *Angew. Chem.* **2007**, *119*, 8747–8750; b) Y. Xie, K. L. Ding, Z. M. Liu, R. T. Tao, Z. Y. Sun, H. Y. Zhang, G. M. An, *J. Am. Chem. Soc.* **2009**, *131*, 6648–6649; c) B. T. Qiao,
- A. Q. Wang, X. F. Yang, L. F. Allard, Z. Jiang, Y. T. Cui, J. Y. Liu, J. Li, T. Zhang, *Nat. Chem.* **2011**, *3*, 634–641; d) X. F. Yang, A. Q. Wang, B. T. Qiao, J. Li, J. Y. Liu, T. Zhang, *Acc. Chem. Res.* **2013**, *46*, 1740–1748.
- [4] X. C. Kang, J. L. Zhang, W. T. Shang, T. B. Wu, P. Zhang, B. X. Han, Z. H. Wu, G. Mo, X. Q. Xing, *J. Am. Chem. Soc.* **2014**, *136*, 3768–3771.
- [5] L. Foppa, J. Dupont, *Chem. Soc. Rev.* **2015**, *44*, 1886–1897.
- [6] a) L. J. Simon, J. G. van Ommen, A. Jentys, J. A. Lercher, *J. Catal.* **2001**, *201*, 60–69; b) C. Vangelis, A. Bouriazos, S. Sotiriou, M. Samorski, B. Gutsche, G. Papadogianakis, *J. Catal.* **2010**, *274*, 21–28; c) M. Zahmakıran, Y. Tonbul, S. Özkar, *Chem. Commun.* **2010**, *46*, 4788–4790.
- [7] a) A. Louloui, J. Michalopoulos, N. H. Gangas, N. Papayannakos, *Appl. Catal. A* **2003**, *242*, 41–49; b) P. G. Savva, K. Goundani, J. Vakros, K. Bourikas, C. Fountzoula, D. Vattis, A. Lycourghiotis, C. Kordulis, *Appl. Catal. B* **2008**, *79*, 199–207; c) M. Chettibi, A. G. Boudjahem, M. Bettahar, *Trans. Metal Chem.* **2011**, *36*, 163–169.
- [8] H. Z. Liu, T. Jiang, B. X. Han, S. G. Liang, Y. X. Zhou, *Science* **2009**, *326*, 1250–1252.
- [9] a) T. R. Cook, Y. R. Zheng, P. J. Stang, *Chem. Rev.* **2013**, *113*, 734–777; b) H. Furukawa, K. E. Cordova, M. O’Keeffe, O. M. Yaghi, *Science* **2013**, *341*, 12301244; c) M. Li, D. Li, M. O’Keeffe, O. M. Yaghi, *Chem. Rev.* **2014**, *114*, 1343–1370.
- [10] a) Z. Y. Gu, X. P. Yan, *Angew. Chem. Int. Ed.* **2010**, *49*, 1477–1480; *Angew. Chem.* **2010**, *122*, 1519–1522; b) A. C. McKinlay, R. E. Morris, P. Horcajada, G. Férey, R. Gref, P. Couvreur, C. Serre, *Angew. Chem. Int. Ed.* **2010**, *49*, 6260–6266; *Angew. Chem.* **2010**, *122*, 6400–6406; c) Y. Q. Lan, H. L. Jiang, S. L. Li, Q. Xu, *Adv. Mater.* **2011**, *23*, 5015–5020; d) K. Lee, W. C. Isley, A. L. Dzubak, P. Verma, S. J. Stoneburner, L. C. Lin, J. D. Howe, E. D. Bloch, D. A. Reed, M. R. Hudson, C. M. Brown, J. R. Long, J. B. Neaton, B. Smit, C. J. Cramer, D. G. Truhlar, L. Gagliardi, *J. Am. Chem. Soc.* **2014**, *136*, 698–704; e) J. W. Liu, L. F. Chen, H. Cui, J. Y. Zhang, L. Zhang, C. Y. Su, *Chem. Soc. Rev.* **2014**, *43*, 6011–6061; f) Y. Y. Liu, A. J. Howarth, J. T. Hupp, O. K. Farha, *Angew. Chem. Int. Ed.* **2015**, *54*, 9001–9005; *Angew. Chem.* **2015**, *127*, 9129–9133.
- [11] a) L. Peng, J. L. Zhang, Z. M. Xue, B. X. Han, J. S. Li, G. Y. Yang, *Chem. Commun.* **2013**, *49*, 11695–11697; b) W. J. Wang, D. Q. Yuan, *Sci. Rep.* **2014**, *4*, 5711–5717.
- [12] a) S. J. Yang, S. Nam, T. Kim, J. H. Im, H. Jung, J. H. Kang, S. Wi, B. Park, C. R. Park, *J. Am. Chem. Soc.* **2013**, *135*, 7394–7397;

- b) J. S. Li, S. L. Li, Y. J. Tang, M. Han, Z. H. Dai, J. C. Bao, Y. Q. Lan, *Chem. Commun.* **2015**, 51, 2710–2713.
- [13] O. M. Yaghi, H. L. Li, T. L. Groy, *J. Am. Chem. Soc.* **1996**, 118, 9096–9101.
- [14] L. Wang, M. T. Li, Z. Y. Huang, Y. M. Li, S. T. Qi, C. H. Yi, B. L. Yang, *J. Power Sources* **2014**, 264, 282–289.
- [15] X. C. Kang, W. T. Shang, Q. G. Zhu, J. L. Zhang, T. Jiang, B. X. Han, Z. H. Wu, Z. H. Li, X. Q. Xing, *Chem. Sci.* **2015**, 6, 1668–1675.
- [16] S. Shamaei, A. R. Abbasi, N. Noori, E. Rafiee, A. Azadbakht, *Colloids Surf. A* **2013**, 431, 66–72.
- [17] H. C. Zhou, J. L. Song, H. L. Fan, B. B. Zhang, Y. Y. Yang, J. Y. Hu, Q. G. Zhu, B. X. Han, *Green Chem.* **2014**, 16, 3870–3875.
- [18] X. C. Meng, H. Y. Cheng, S. Fujita, Y. F. Hao, Y. J. Shang, Y. C. Yu, S. X. Cai, F. Y. Zhao, M. Arai, *J. Catal.* **2010**, 269, 131–139.
- [19] A. P. Umpierre, E. de Jesús, J. Dupont, *ChemCatChem* **2011**, 3, 1413–1418.
- [20] I. N. Remediakis, N. Lopez, J. K. Nørskov, *Angew. Chem. Int. Ed.* **2005**, 44, 1824–1826; *Angew. Chem.* **2005**, 117, 1858–1860.

Received: August 30, 2015

Revised: October 16, 2015

Published online: November 30, 2015